Catalysis Today 164 (2011) 467–473

Contents lists available at ScienceDirect

Catalysis Today

journal homepage: www.elsevier.com/locate/cattod

Characterization and dynamic behavior of precious metals in automotive exhaust gas purification catalysts

Hirohito Hirata[a,*], Keisuke Kishita[b], Yasutaka Nagai[c], Kazuhiko Dohmae[c], Hirofumi Shinjoh[c], Shin'ichi Matsumoto[d]

[a] Toyota Motor Corporation, Advanced Material Engineering Div., 1200, Mishuku, Susono, Shizuoka 410-1193, Japan
[b] Toyota Motor Corporation, Material Engineering Management Div., 1, Toyota-cho, Toyota, Aichi 471-8572, Japan
[c] Toyota Central R&D Labs. Inc., Nagakute, Aichi 480-1192, Japan
[d] Toyota Motor Corporation, Power Train Material Engineering Div., 1, Toyota-cho, Toyota, Aichi 471-8572, Japan

ARTICLE INFO

Article history:
Received 29 June 2010
Received in revised form 3 November 2010
Accepted 3 November 2010
Available online 3 December 2010

Keywords:
Platinum
Rhodium
Sintering
Three-way catalyst
In situ XAFS
In situ TEM

ABSTRACT

Both the behaviors of sintering and reactivation of Pt and Rh on various metal oxide supports were investigated by TEM, CO pulse chemisorption and XAFS analysis. The results suggest that phenomenon of reversible sintering and re-dispersion to reduced, active metallic sites is related to the electron density of O atoms in support and to the crystal structure of support.

As a result of *in situ* XAFS and *in situ* TEM analysis, Pt reversible sintering and re-dispersion phenomenon was observed on CeO2 based metal oxide. The Pt re-dispersion process proceeds by the repetition of (1) migration of Pt oxide from the surface of large Pt particles, (2) adsorption of Pt oxide on the surface of CeO_2 based metal oxide by strong Pt–O–Ce interaction and (3) reduction Pt oxide and Pt–O–Ce bond.

To achieve a good balance between activity and the sintering suppression, CeO_2 based metal oxide is selected as Pt support, and ZrO_2 is used as Rh support. The blended catalyst of Pt on ceria based oxide and Rh on ZrO_2 has higher activity after aging.

1. Introduction

Recently, for the purpose of purifying carbon monoxide (CO), hydrocarbons (HC) and nitrogen oxides (NO_x) in automotive exhaust, a three-way catalyst is absolutely necessary and indispensable for every gasoline fueled vehicle. It decreases the emission of these pollutants drastically, however even more improvement is needed in order to meet the stringent emission restrictions planned for the near future.

One of the biggest issues for three-way catalysts is the degradation of catalytic activity caused by sintering of precious metals which serve as active sites [1–4]. Several strategies have been employed with the goal of improving the activity of the catalyst after aging: improving precious metal dispersion with high surface area supports, adding promoters, and improving the thermal stability of these supports and promoters, etc. [5–11]. However, there are currently no established methods for suppressing precious metals sintering and this has resulted in the use of large quantities of noble metals for catalysts to meet the stringent emission standards. As precious metals are very scarce resources, their consumption should be reduced.

Through the investigation of the sintering behavior of precious metals on different support oxides, it was found that some supports could efficiently suppress precious metal sintering via an anchoring effect on the supports. In this paper, the sintering behavior and sintering suppression mechanism of precious metals (Pt and Rh) on various metal oxide supports are discussed and summarized. The activity of new catalysts developed on the basis of the sintering suppression concept is also presented here.

In this research, in order to elucidate the sintering behavior and reactivation of precious metals, we conducted a systematic investigation of precious metal sintering on various metal oxide supports. The physical change of precious metal particle size after aging treatment was measured by TEM and CO pulse chemisorption and then correlated with the binding energy of O(1s) electrons in the oxides as measured by XPS. The local structure around the precious metal atoms was analyzed by EXAFS. Furthermore, in order to understand the behavior of Pt particles under real exhaust conditions, flowing *in situ* dynamic observation of *in situ* XAFS and *in situ* TEM under simulated condition were performed.

2. Experimental

2.1. Sample preparation and aging treatment

Preparation of 2 wt% Pt/Al_2O_3 and 2 wt% Pt/CZY catalysts was done by the conventional wet impregnation of Al_2O_3 and

* Corresponding author. Tel.: +81 55 997 7835; fax: +81 55 997 7879.
E-mail address: hirata@hirohito.tec.toyota.co.jp (H. Hirata).

0920-5861/$ – see front matter © 2010 Elsevier B.V. All rights reserved.
doi:10.1016/j.cattod.2010.11.005

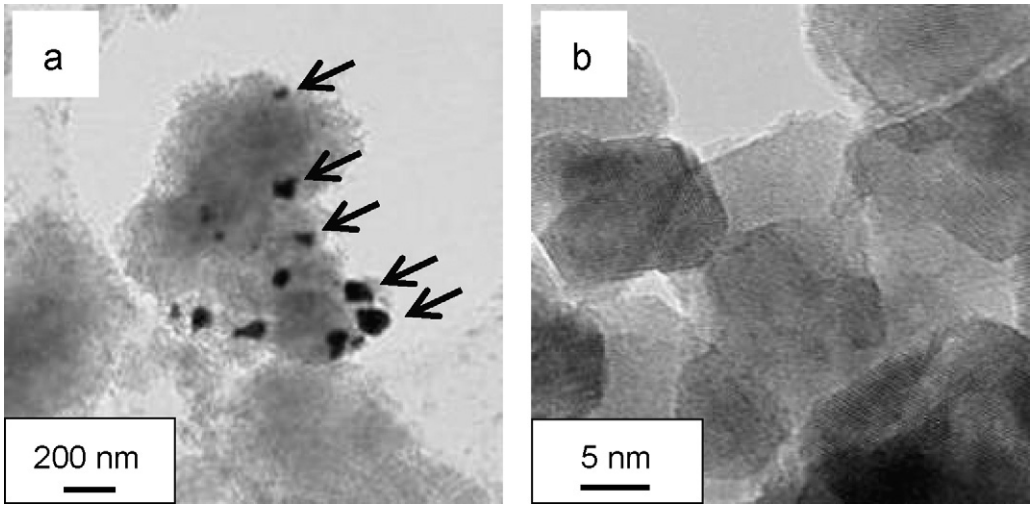

Fig. 1. TEM images of Pt supported catalysts after 800 °C aging in air for 5 h. (a) Pt/Al_2O_3 catalyst. (b) Pt/CZY (CZY denotes Ce–Zr–Y mixed oxide) catalyst. The arrows indicate the position of large Pt particles.

CZY (50 wt% CeO_2, 46 wt% ZrO_2, and 4 wt% Y_2O_3) powders with $Pt(NH_3)_2(NO_2)_2$ aqueous solution. The impregnated powders were dried overnight at 110 °C and calcined at 500 °C for 3 h in air. These samples are referred to as "fresh catalysts." Portions of the fresh sample were aged in air for 5 h at 800 °C. This aging treatment corresponds to an accelerated test for durability in an oxidative atmosphere. These samples are referred to as "aged catalysts." Pt/SiO_2, Pt/ZrO_2, Pt/TiO_2, and Pt/CeO_2 for a systematic study were prepared by the aforementioned method, using commercial support oxides, and aged as described above.

Preparation of 0.5 wt% Rh loaded catalysts was done using the same procedure as the Pt catalyst, however $Rh(NO_3)_3$ aqueous solution was used instead of $Pt(NH_3)_2(NO_2)_2$. Regarding the metal oxide supports, SiO_2, Al_2O_3, ZrO_2, YZ (3 wt% Y_2O_3 doped ZrO_2), and CeO_2 were used. Portions of the fresh sample were aged in air for 5 h at 1000 °C.

2.2. Characterization

The average particle size of Pt metal was determined using a CO pulse adsorption method [12]. The catalysts were pretreated in flowing pure oxygen, followed by pure hydrogen at 400 °C. The CO pulse adsorption was carried out in flowing He at −78 °C [13]. At this temperature, CO uptake on ceria was almost entirely suppressed, and CO was adsorbed only on the surface of Pt. The average particle size was calculated from the CO uptake assuming that CO was adsorbed on the surface of spherical Pt particles at a stoichiometry of CO/(surface Pt atom) = 1/1.

In the case of the Rh catalysts, the samples were pretreated in flowing pure oxygen, followed by pure hydrogen at 400 or 700 °C. The average particle size was calculated using an adsorption ratio of CO/(surface Rh atom) = 1.4/1. The remainder of measurement procedure was same as for Pt.

The microstructure of the catalysts was investigated by transmission electron microscopy (TEM) using a JEOL JEM-2000EX.

The Pt L3-edge or Rh K-edge X-ray absorption fine structure (XAFS) measurement was carried out at BL01B1 and BL16B2 of SPring-8 (Hyogo, Japan) [14,15]. The storage ring energy was operated at 8 GeV with a typical current of 100 mA.

The X-ray photoelectron spectroscopy (XPS) measurements were carried out using a PHI model 5500MC with Mg Kα X-rays.

2.3. In situ dynamic observation

In situ XAFS measurements, Pt L3-edge XANES spectra were measured every 1–6 s at ESRF ID24. 3% H_2 (He balance) and 20% O_2 (He balance) gases were introduced to the *in situ* sample cell alternately every 60 s at 600 °C [16]. *In situ* TEM observation was carried out on a specially modified Hitachi model-9500 300 kV HR-TEM at Toyota, Japan [17]. The *in situ* experiments involved the sample being exposed to either vacuum (below 10^{-5} Pa) or 1 Pa O_2 injections at 750 °C.

3. Results and discussion

3.1. Analysis of Pt sintering on various metal oxide support

Fig. 1 shows the TEM images of the Pt/Al_2O_3 and Pt/CZY catalysts after an aging treatment at 800 °C in air for 5 h. In the aged Pt/Al_2O_3 sample, large Pt particles ranging from 3 to 150 nm were observed. In contrast, no distinct Pt particles were observed on the aged Pt/CZY sample. In the aged Pt/CZY sample, Pt was detected by EDX analysis. This indicates that Pt particles are highly dispersed on the CZY support.

The average Pt particle size on the Al_2O_3 support increased significantly from 1.0 to 23.6 nm due to the aging treatment. On the other hand, Pt particles on Pt/CZY maintained a size of 1.1 nm before and after aging. This indicates that Pt in the Pt/CZY catalyst did not sinter at all after the aging treatment.

The Fourier transformed Pt L3-edge EXAFS spectra of the aged catalysts and reference samples are shown in Fig. 2. For the aged Pt/Al_2O_3 sample, only an intense peak which corresponds to the Pt–Pt bond was observed. The spectrum of the Pt/Al_2O_3 coincides with that of Pt foil. This indicates that large Pt metal particles exist on the Al_2O_3 surface [18].

For the aged Pt/CZY sample, two peaks were observed. The first peak at 1.7 Å is assigned to the Pt–O bond by comparison to a PtO_2 reference. The second peak at 2.7 Å was not observed in either the Pt foil or the PtO_2 sample. As a result of careful analysis, this peak is assigned as the Pt–O–Ce bond [14]. In addition, intense Pt–Pt or Pt–O–Pt peaks could not be observed in the aged Pt/CZY sample, suggesting that there are no large Pt metal or oxide particles on the CZY surface. In other words, highly dispersed Pt oxides are present on the surface of CZY.

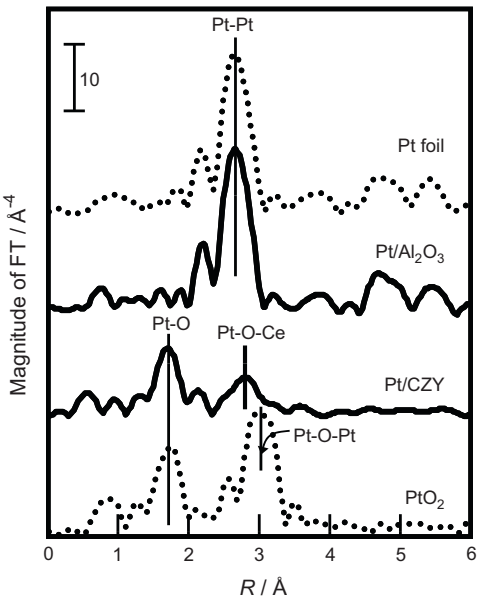

Fig. 2. Fourier-transformed k^3x data of Pt L3-edge EXAFS for supported Pt catalysts after 800 °C aging in air as compared to standard samples of Pt foil and PtO_2 powder.

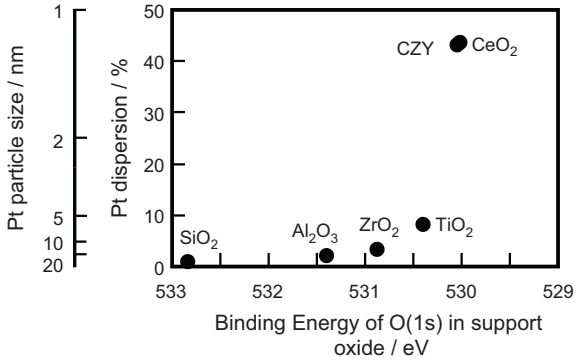

Fig. 3. Pt–oxide-support interaction and its relation to Pt sintering in an oxidizing atmosphere.

Based on the observation above, the sintering inhibition mechanism of Pt supported on CZY is proposed as follows. In the case of Pt/Al_2O_3, since the interaction between Pt and Al_2O_3 is weak, mobile Pt particles migrate across the surface of the Al_2O_3 support and sinter during an 800 °C aging treatment in an oxidizing atmosphere. In contrast, Pt supported on CZY has a strong interaction with the CZY support. Therefore, the CZY support stabilizes a high-oxidation state of Pt, and then the formation of the rigid Pt–O–Ce bond acts as an anchor. The formation of the Pt–O–Ce bond on the CZY suppresses the sintering of Pt.

The average size of the Pt metal particles after the aging treatment on SiO_2, Al_2O_3, ZrO_2, TiO_2, CeO_2 and CZY was estimated using the CO pulse method. In addition, the binding energy of the O(1s) electron in those support oxides was measured by XPS. The binding energy of O(1s) relates to electron density of the support. Fig. 3 shows the relationship between the binding energy of the O(1s) electron and the Pt particle size after aging. The Pt particle size after aging decreases as the electron density of oxygen increases. This implies that the sintering inhibition effect on Pt can be controlled by the electron density of the support oxide through the Pt–O–M bond. That is the key parameter of the Pt–oxide-support interaction and its relation to Pt sintering in an oxidizing atmosphere.

Generally, Pt^0 (metal) is considered to be the active site for the catalytic reaction under automotive exhaust conditions. The CZY support can stabilize the oxidation state of Pt after aging. Therefore, Pt on the CZY support must be reducible during the catalytic reaction. The result of CO pulse experiments suggests that Pt on CZY is reduced under pretreatment condition (400 °C reduction). Furthermore, our previous investigation of the local structure of Pt atoms on oxidized Pt/CZY and reduced Pt/CZY by XAFS showed that Pt on CZY changes to the metallic state after the reducing treatment [14].

On the basis of these analysis results, CeO_2–ZrO_2 mixed oxide (CZY) is selected as the most suitable support for Pt.

3.2. In situ dynamic observation of Pt sintering and re-dispersion on CZY

The exhaust gas condition from a gasoline engine changes quickly and dramatically in response to the driver's operation. The temperature can reach levels up to 1000 °C and the gas condition changes between oxidative and reductive atmosphere. Fig. 4 shows TEM images of Pt/CZY after aging treatment under oxidizing or reducing atmosphere. For the catalyst aged under oxidizing atmosphere, Pt particles were not observed. In this case, the average Pt particle size as measured by CO pulse was 1.1 nm. On the other hand, for the catalyst aged under reducing atmosphere, Pt parti-

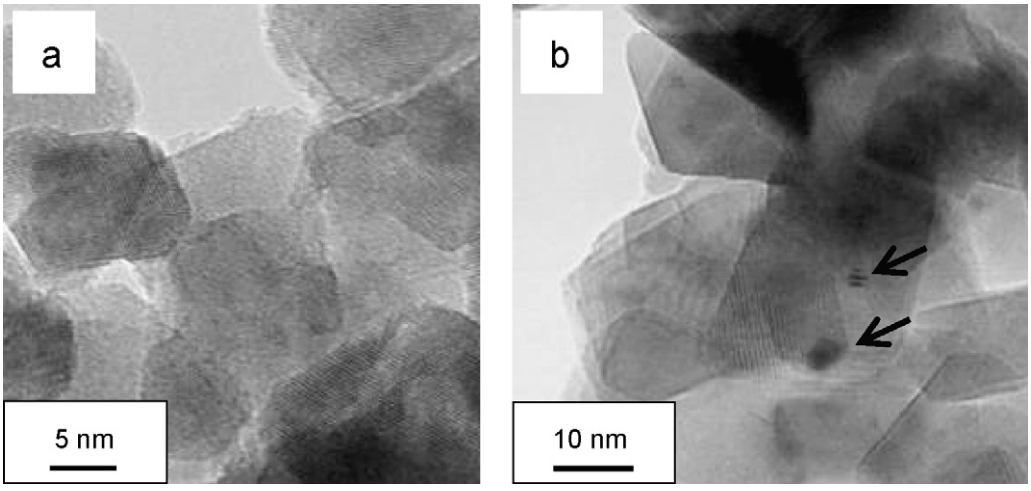

Fig. 4. TEM images of Pt/CZY catalysts. (a) After 800 °C aging in air for 5 h. (b) After 1000 °C aging in reducing atmosphere for 5 h. The arrows indicate the position of Pt particles.

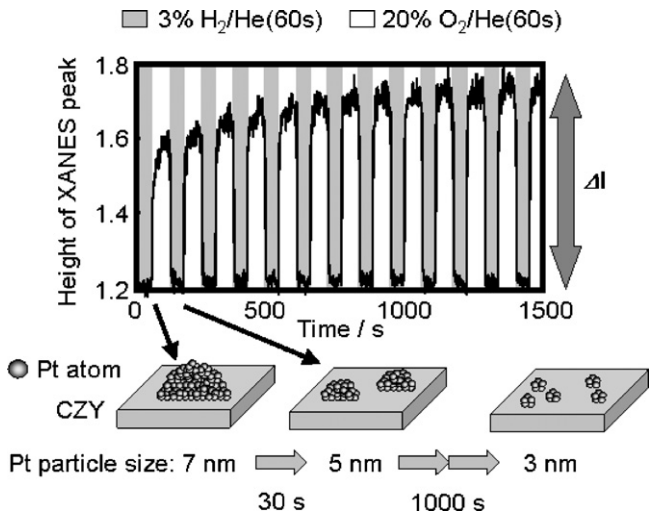

Fig. 5. The height of XANES peak for the sintered Pt/CZY catalyst as a function of time and gas condition and the schematic representation of the re-dispersion behavior.

cles were observed and the average Pt particle size as measured by CO pulse was 7 nm. In order to observe influence of changing gas conditions on Pt/CZY, *in situ* dynamic observation by XAS and TEM were employed.

Fig. 5 shows the white-line peak height of the normalized Pt L3-edge XANES for the sintered Pt/CZY catalyst. The data was collected every 1 s. The white-line peak height changes very quickly, within 1 s, between the values of reduced and that of oxidized Pt after switching the gas atmosphere. This result indicates that the reduction and oxidation of Pt is very fast. While the white-line peak height under the reducing atmosphere is constant, the height under the oxidizing atmosphere increases gradually. The difference between the white-line peak height of the oxidized and reduced samples corresponds with the particle size of Pt [18]. Using the relationship between Pt particle size and difference of white-line peak height [18], we estimate Pt particle size under *in situ* observation. The Pt particle size of the aged catalyst decreased from 7 to 5 nm after 60 s, and then to 3 nm after 1000 s. This kind of Pt redispersion was not observed in a conventional Pt/Al_2O_3 catalyst. These results suggest that the Pt particles on CZY are easily oxidized under the 20% O_2 gas stream, the newly formed Pt oxide migrates and is trapped on the surface of CZY through the strong Pt–ceria support interaction. After that the gas condition changes to the reducing atmosphere, the trapped Pt ions (Pt^{2+} or Pt^{4+}) assemble into smaller Pt metal particles.

In order to verify our interpretation of the *in situ* XAS measurements, *in situ* TEM observations were performed on the Pt/CZY sample. Fig. 6 shows snapshots of *in situ* TEM experiments on aged Pt/CZY. In initial state, the size of Pt particle is about 7 nm. After 1 Pa O_2 injection, the Pt particle size changes to about 2 nm. When the atmosphere changes to vacuum (effectively a reducing condition)

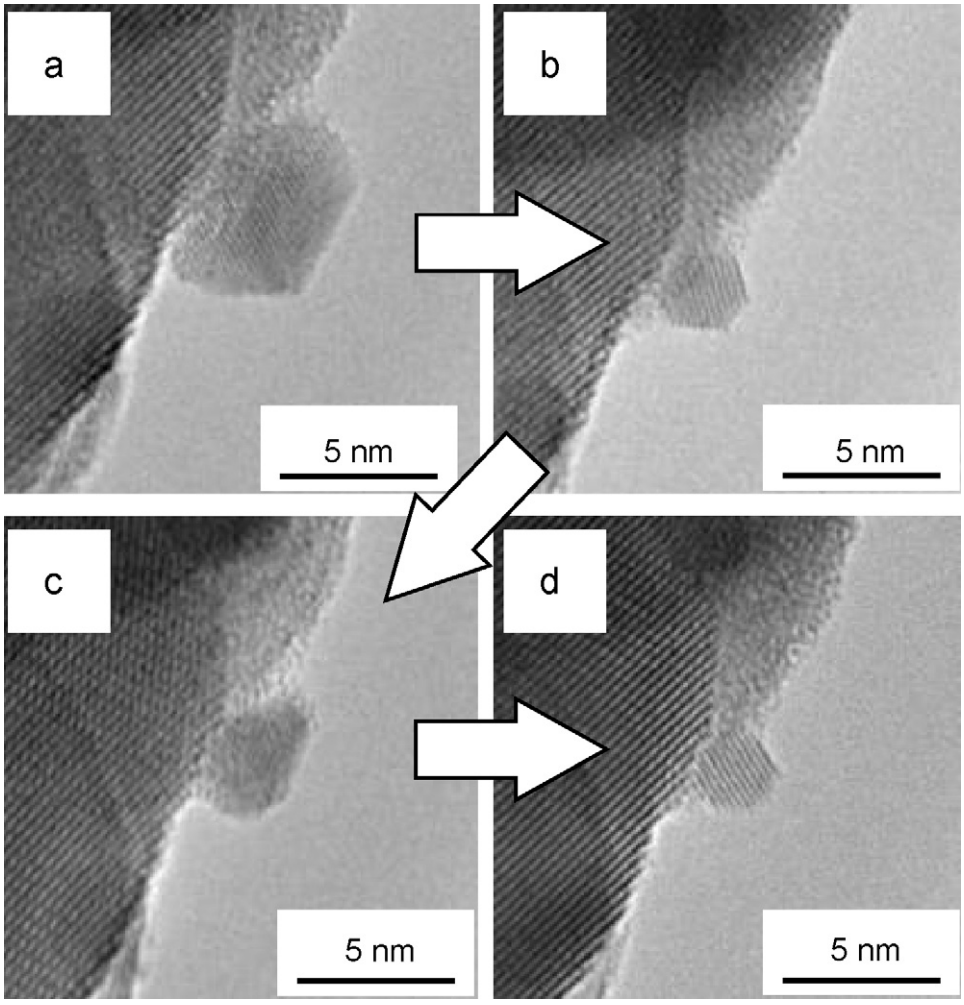

Fig. 6. *In situ* TEM images of the Pt re-dispersion process on Pt/CZ at 750 °C. (a) Vacuum, (b) 1 Pa O_2, (c) vacuum, (d) 1 Pa O_2.

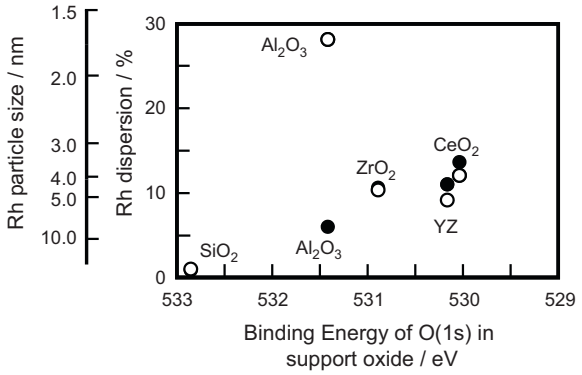

Fig. 7. Rh–oxide support interaction and its relation to Rh sintering in an oxidizing atmosphere. •: Pretreated at 400 °C under reducing conditions, ○: pretreated at 700 °C under reducing conditions.

the size of Pt particle increases to approximately the original size of about 7 nm. After repeating the 1 Pa O_2 injection the Pt particle size again reduces to about 2 nm. This result is consistent with the *in situ* XAS measurements and suggests reversible sintering and re-dispersion can be initiated by controlling the atmosphere.

3.3. Analysis of Rh sintering on various metal oxide support

For the analysis of the Rh-based catalysts, the same suite of experiments was performed as in the previous study of Pt catalysts [15].

Fig. 7 shows the relationship between the binding energy of the O(1s) electron and the average size of the Rh metal particles after the aging treatment. Basically, the average Rh particle size after aging decrease as the electron density of oxygen increases. The average Rh particle size on SiO_2, ZrO_2, YZ and CeO_2 maintained almost same size despite the change in pretreatment temperature from 400 to 700 °C. On the other hand, the average Rh particle size on Al_2O_3 changed drastically after the high temperature treatment. This suggests that in case of Rh/Al_2O_3 another factor affects Rh sintering inhibition.

Fig. 8 show the TEM images of Rh/SiO_2, Rh/Al_2O_3, Rh/ZrO_2 and Rh/CeO_2 catalysts after an aging treatment at 1000 °C in air for 5 h. In case of aged Rh/SiO_2, Rh/ZrO_2 and Rh/CeO_2, Rh particles were observed. In contrast, Rh particles were not observed on aged Rh/Al_2O_3. However, after 800 °C reduction treatment Rh particles appeared on Al_2O_3 (Fig. 8b′).

In order to analyze local structure around the Rh atoms, EXAFS spectra were collected. The Fourier transformed Rh K-edge EXAFS spectra of the aged catalysts and reference samples are shown in Fig. 9. The spectrum of aged Rh/SiO_2 is similar to the reference Rh_2O_3 spectrum. This indicates that large Rh_2O_3 particles exist on the surface of SiO_2. For the aged Rh/ZrO_2, only one weak peak at 1.6 Å was observed. This peak is assigned to the Rh–O bond by comparison to the Rh_2O_3 reference. The weakness of the Rh–O peak intensity and the absence of the Rh–O–Rh peak at 2.7 and 3.3 Å suggest that small Rh oxide particles exist on CeO_2 surface.

In case of aged Rh/Al_2O_3, two peaks were observed. The first peak at 1.6 Å is assigned to the Rh–O bond peak. The second peak at around 2.5–3.0 Å was not observed in either the Rh foil or the Rh_2O_3 sample. This peak is assigned as the Rh–O–Al peak. This indicates a strong interaction exists between Rh and Al through O atom [15]. Weng-Sieh et al. showed that Rh forms hexagonal Rh_2O_3 in an oxidizing atmosphere above 650 °C which results in epitaxial stabilization of hexagonal Rh_2O_3 on Al_2O_3 [19,20]. On the basis of analytical results and previous knowledge, we believe that Rh supported on Al_2O_3 diffuses into the Al_2O_3 lattice where it is stabilized by the strong Rh–O–Al bond. In this case, this chemical and structural interaction affects the Rh behavior on Al_2O_3.

As is the case with Pt, Rh^0 (metal) is considered to be the active site for the catalytic reaction under automotive exhaust conditions. The results of CO pulse and TEM observation suggest that the interaction between Rh and Al is too strong to reduce the oxidized Rh back to its metallic state using the current reducing treatment. The aged Rh/Al_2O_3 needs a higher temperature reduction to form metallic Rh on Al_2O_3 compared to other supported Rh catalysts.

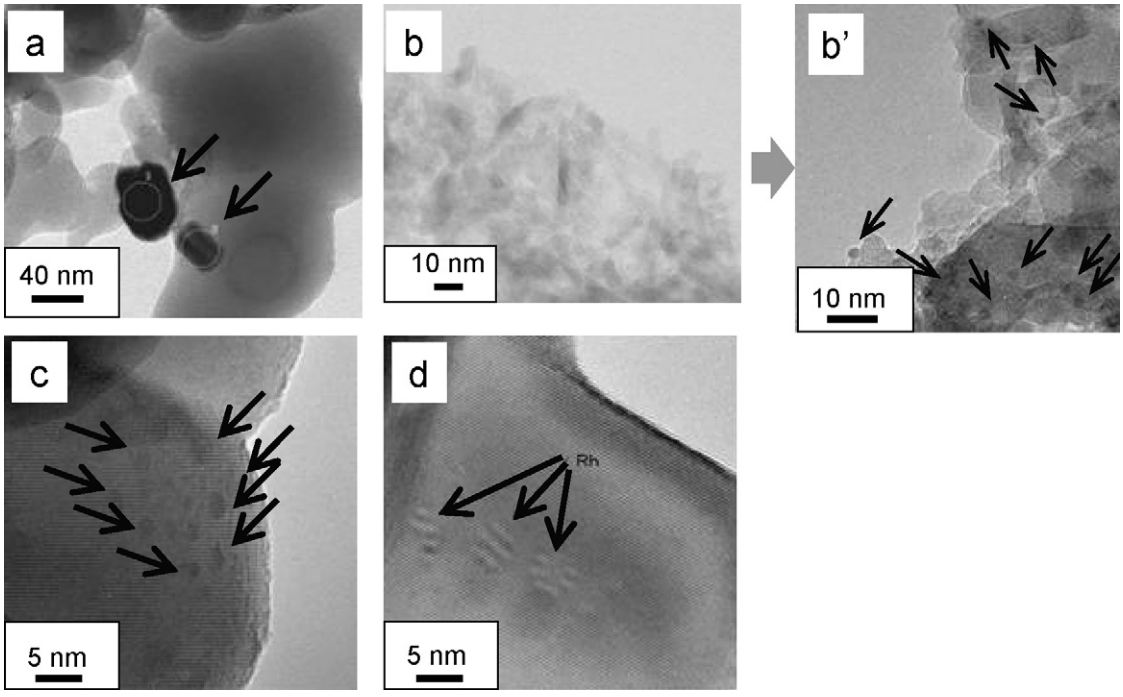

Fig. 8. TEM images of Rh supported catalysts after 1000 °C aging in air for 5 h. (a) Rh/SiO_2, (b) Rh/Al_2O_3, (c) Rh/ZrO_2, and (d) Rh/CeO_2. (b′) After 800 °C reduction treatment of (b). The arrows indicate the position of Rh particles.

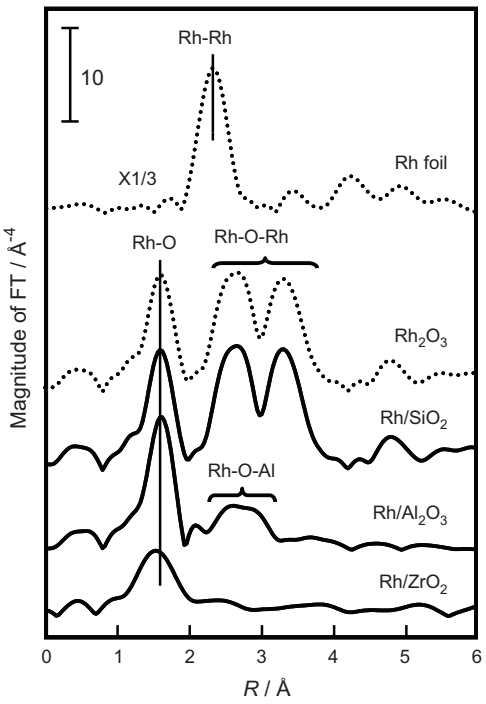

Fig. 9. Fourier-transformed k^3x data of Rh K-edge EXAFS for supported Rh catalysts after 1000 °C aging in air as compared to standard samples of Rh foil and Rh_2O_3 powder.

In our previous study of Pt/MgO showed the strong Pt–O–Mg bond suppress Pt sintering, however this strong Pt–O–Mg bond is difficult to decompose to change active metallic Pt by reducing treatment [21]. These results suggest too strong interaction between active site and support is not suitable for reactivation of catalyst.

On the basis of these analysis results, CeO_2 and ZrO_2 are selected as the most suitable support for Rh.

3.4. Development of new catalyst

On the basis of previous results, three types of catalysts were prepared. Catalyst A, Pt and Rh coexisted on a ceria based oxide; catalyst B, blend of Pt and Rh supported separately on a ceria based oxide; and catalyst C, blend of Pt on ceria based oxide and Rh on ZrO_2. The total amount of Pt and Rh on each catalyst was same.

The catalytic activities of the three catalysts after an aging test at 1000 °C are shown in Fig. 10 [22]. The catalyst C exhibited the best activity. We suggest that the reason is as follows: (1) the oxidation state of Rh on ZrO_2 is more metallic compared to on ceria based metal oxides because the electron density of oxygen for ZrO_2 is lower than for ceria based oxide, (2) Pt and Rh sintering are efficiently suppressed by their own matched metal–support interactions.

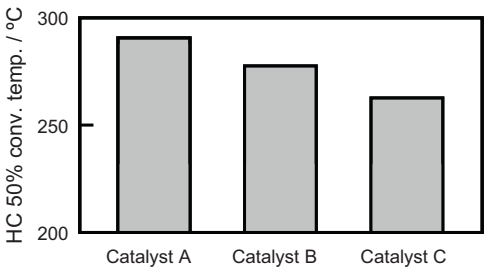

Fig. 10. Catalytic activities after aging test at 1000 °C.

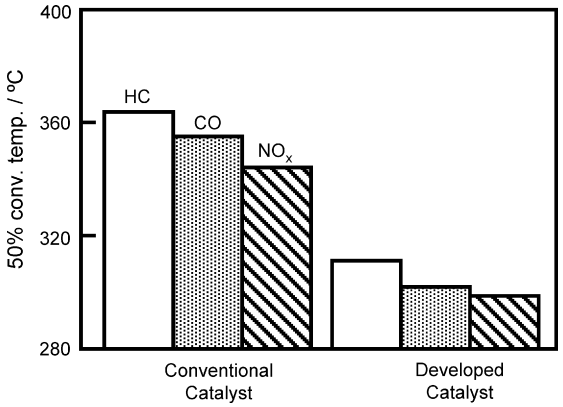

Fig. 11. Performance of the developed catalyst in engine bench test after the engine aging.

Based on the concept of the support anchoring effect, a new 3-way catalyst (monolithic catalyst) was designed. Pt and Rh were separately and respectively loaded on CeO_2-based and ZrO_2-based oxides. Fig. 11 shows the catalytic activity of the developed catalyst based on an engine test after aging [23]. Compared to the conventional catalyst, this developed catalyst showed a higher catalytic activity.

4. Conclusion

Pt particle size after aging depends on the electron density of oxygen in the support and Pt-support interaction is the key to sintering inhibition. CZY (CeO_2–ZrO_2–Y_2O_3) is a better support for Pt.

The result of *in situ* dynamic observations suggest the presence of reversible Pt sintering and re-dispersion on CZY. The driving force of this Pt re-dispersion is attributed to the strong Pt–O–Ce interaction that forms under oxidizing atmosphere.

Rh particle size after aging depends on electron density of oxygen in support and structural interaction (e.g. Rh diffuse into support Al_2O_3). ZrO_2 is a better support for Rh.

On the basis of these analysis results, a new 3-way catalyst was developed. The blended catalyst of Pt on ceria based oxide and Rh on ZrO_2 has higher activity after aging. This suggests the optimization of the metal–support interaction is useful for improvement of catalyst durability.

Acknowledgments

The authors thank all researchers at ESRF, Toyota Motor Europe, Toyota Central R&D Labs. and Toyota Motor Corporation who relate to this research.

References

[1] P.J.F. Harris, J. Catal. 97 (1986) 527.
[2] R.M.J. Fiedorow, B.S. Chahar, S.E. Wanke, J. Catal. 51 (1978) 193.
[3] C.H. Bartholomew, Appl. Catal. A 212 (2001) 17.
[4] H. Birgersson, L. Eriksson, M. Boutonnet, S.G. Järås, Appl. Catal. B 54 (2004) 193.
[5] S. Matsumoto, Catal. Today 90 (2004) 183.
[6] H.C. Yao, Y.F. Yao, J. Catal. 86 (1984) 254.
[7] M. Ozawa, M. Kimura, A. Isogai, J. Alloys Compd. 193 (1993) 73.
[8] T. Kanazawa, J. Suzuki, T. Takada, T. Suzuki, A. Morikawa, A. Suda, H. Sobukawa, M. Sugiura, SAE Paper No. 2003-01-087, 2003.
[9] N. Miyoshi, S. Matsumoto, M. Ozawa, M. Kimura, SAE Paper No. 891970, 1989.
[10] M. Ozawa, M. Kimura, A. Isogai, J. Less-Common Met. 162 (1990) 297.
[11] F. Oudet, P. Courtine, A. Vejux, J. Catal. 114 (1988) 112.
[12] T. Uchijima, Catalytic Science and Technology, Kodansha–VCH, Weinheim, 1990.

[13] A. Holmgren, B. Andersson, D. Duprez, Appl. Catal. B 22 (1999) 215.
[14] Y. Nagai, T. Hirabayashi, K. Dohmae, N. Takagi, T. Minami, H. Shinjoh, S. Matsumoto, J. Catal. 242 (2006) 103.
[15] Y. Nagai, K. Domae, N. Takagi, T. Hirabayashi, T. Minami, N. Takahiashi, H. Shinjoh, S. Matsumoto, Sahokubai 52 (2010) 149.
[16] Y. Nagai, K. Dohmae, Y. Ikeda, N. Takagi, T. Tanabe, N. Hara, G. Guilera, S. Pascarelli, M.A. Newton, O. Kuno, H. Jiang, H. Shinjoh, S. Matsumoto, Angew. Chem. Int. Ed. 47 (2008) 9303.
[17] K. Kishita, H. Sakai, H. Tanaka, H. Saka, K. Kuroda, M. Sakamoto, A. Watabe, T. Kamino, J. Electron Microsc. 54 (2009) 331.
[18] Y. Nagai, N. Takagi, Y. Ikeda, K. Dohmae, T. Tanabe, S. Pascarelli, G. Guilera, M. Newton, H. Shinjoh, S. Matsumoto, PI-439, TOCAT5, Tokyo, Japan, 2006.
[19] Z. Weng-Sieh, R. Gronsky, A.T. Bell, J. Catal. 170 (1997) 62.
[20] Z. Weng-Sieh, R. Gronsky, A.T. Bell, J. Catal. 174 (1998) 22.
[21] Y. Nagai, K. Dohmae, K. Teramura, T. Tanaka, G. Guilera, K. Kato, M. Nomura, H. Shinjoh, S. Matumoto, Catal. Today 145 (2009) 279.
[22] H. Shinjoh, M. Hatanaka, Y. Nagai, T. Tanabe, N. Takahashi, T. Yoshida, Y. Miyake, Topics Catal. 52 (2009) 1967.
[23] T. Yoshida, A. Sato, H. Suzuki, T. Tanabe, N. Takahashi, SAE Paper No. 010161, 2006.